

On the role of the baroclinic torque on surface gravity wave propagation^{a)}Eyal Heifetz¹, Ron Maor¹ and Anirban Guha^{2,3}¹Department of Geophysics, Porter school of the Environment and Earth Sciences, Tel-Aviv University, Israel.²Mechanical Engineering Department, Indian Institute of Technology Kanpur, India.³ Institute of Coastal Research, Helmholtz-Zentrum Geesthacht, Geesthacht, Germany.

(Dated: 27 March 2022)

Surface gravity waves are one of the most fundamental phenomena in ocean dynamics, yet the standard potential flow approach to derive its dispersion relation seems to obscure the mechanistic understanding of the wave propagation and the dependence of the dispersion relation on the wavenumber. Here we provide an alternative derivation, based solely on the vortex sheet dynamics at the air-water interface. We show how the two terms of the baroclinic torque operate to translate the interfacial vorticity anomalies and how the non-Boussinesq term of the baroclinic torque acts against the Boussinesq one to hinder the wave propagation. We further investigate, via vorticity inversion approach, how the existence of the bottom boundary affects the propagation mechanism by replacing this boundary by an anti-phased vortex sheet mirror image. The limits of deep and shallow-water dynamics are discussed as well from this perspective. Furthermore, solely from the interface dynamics, we show the validity of the Virial theorem for surface gravity waves.

PACS numbers: 47.20.Ma,47.15.St,47.20.Ft

Keywords: surface gravity waves, vortex sheet

^{a)}Corresponding author address: Anirban Guha. Email: anirbanguha.ubc@gmail.com

I. INTRODUCTION

The theory of linear surface gravity waves has been founded in the eighteenth and the early nineteenth century by pioneers like Laplace, Lagrange, Poisson, and Cauchy¹. The standard derivation of the dispersion relation, based on the potential flow theory, is a well known procedure considered in almost all standard textbooks in fluid dynamics (e.g. Kundu, Cohen, and Dowling²). In this derivation, however, the implementation of the kinematic and dynamic conditions (the latter via the time-dependent Bernoulli equation) seems to obscure the physical mechanism of the wave propagation and the reason for the peculiar dispersion relation $\omega(k) = \pm\sqrt{gk \tanh(kH)}$ (where ω denotes frequency, g is gravity, k is the wavenumber and H is the water depth).

In recent times, there has been a growing body of literature^{3–10} dealing with stratified shear flow instability that treats the dynamics of density discontinuity surfaces as *interfacial vorticity waves*¹¹. This approach provides a mechanistic rationalization for Taylor-Caulfield and Holmboe instabilities, and also paves the path for efficient vortex-method-based computation schemes to simulate the nonlinear evolution, including wave-breaking¹². However, while exploring these relatively complex problems, the analysis of surface gravity waves - probably the simplest setup of a discontinuous surface - in terms of interfacial vorticity waves has been “left behind”. Hence, here we suggest an alternative derivation of surface gravity waves, based on the above-mentioned approach.

This article is organized as follows. In Sec. II, we derive and analyze the interfacial vorticity equations and then in Sec. III, we implement them to obtain the dispersion relation. Special care is given to the deep and shallow-water limits. In Sec. IV we derive surface waves’ energy from the interfacial fields. Finally, we close by discussing the results in Sec. V.

II. INTERFACIAL VORTICITY DYNAMICS

The governing incompressible continuity and Navier-Stokes equations of an inviscid, non-diffusive density stratified fluid are:

$$\nabla \cdot \mathbf{u} = 0, \quad \frac{D\rho}{Dt} = 0, \quad (2.1a,b)$$

$$\frac{D\mathbf{u}}{Dt} = -g\hat{\mathbf{k}} - \frac{1}{\rho}\nabla p. \quad (2.1c)$$

Here $D/Dt \equiv \partial/\partial t + \mathbf{u} \cdot \nabla$ is the material derivative, and \mathbf{u} , ρ , p and g respectively denote velocity, density, pressure and acceleration due to gravity. Furthermore, $\hat{\mathbf{k}}$ is a unit vector pointing in a direction opposite to gravity. The vorticity equation can be obtained by taking the curl of Eq. (2.1c) and using Eq. (2.1a,b):

$$\frac{D\mathbf{q}}{Dt} = \underbrace{(\mathbf{q} \cdot \nabla)\mathbf{u}}_{\text{Stretching}} + \underbrace{\frac{1}{\rho^2} \nabla \rho \times \nabla p}_{\text{Baroclinic}}, \quad (2.2)$$

where $\mathbf{q} \equiv \nabla \times \mathbf{u}$ is the vorticity. The first term on the RHS is the vortex stretching term that would be absent in 2D flows. The second term signifies the baroclinic generation of vorticity – vorticity generated when the isopycnals and isobars are not parallel. In general, this term can be divided into two parts – *Boussinesq* and *non-Boussinesq*.

Since our interest is on surface gravity waves, we consider the simpler and more familiar 2D (x, z) setup of hydrostatic background:

$$\frac{d\bar{p}}{dz} = -\bar{\rho}g, \quad (2.3)$$

where \bar{p} is the mean pressure and $\bar{\rho}$ is the mean density. On linearizing the governing Navier-Stokes equations (2.1c) about the hydrostatic base state, we obtain

$$\frac{\partial u'}{\partial t} = -\frac{1}{\bar{\rho}} \frac{\partial p'}{\partial x}, \quad (2.4a)$$

$$\frac{\partial w'}{\partial t} = -\frac{1}{\bar{\rho}} \frac{\partial p'}{\partial z} - \frac{\rho'}{\bar{\rho}} g. \quad (2.4b)$$

The conservation of mass gives rise to

$$\frac{\partial \rho'}{\partial t} = -w' \frac{d\bar{\rho}}{dz}, \quad (2.4c)$$

$$\frac{\partial u'}{\partial x} + \frac{\partial w'}{\partial z} = 0. \quad (2.4d)$$

In Eqs. (2.4a)–(2.4d), the primes denote perturbation quantities. Hereafter, the primes will be dropped for simplicity; any variable without overbar will denote perturbation quantity.

Defining the 2D vorticity (q points in the negative y direction; we follow the convention in which counterclockwise (clockwise) rotation is associated with positive (negative) values of vorticity) perturbation as

$$q = \frac{\partial w}{\partial x} - \frac{\partial u}{\partial z}, \quad (2.5)$$

the 2D version of Eq. (2.2) yields

$$\frac{\partial q}{\partial t} = \underbrace{-\frac{g}{\bar{\rho}} \frac{\partial \rho}{\partial x}}_{T_1 \equiv \text{Boussinesq baroclinic}} + \underbrace{\left[-\frac{1}{\bar{\rho}^2} \left(\frac{d\bar{\rho}}{dz} \frac{\partial p}{\partial x} \right) \right]}_{T_2 \equiv \text{Non-Boussinesq baroclinic}}. \quad (2.6)$$

The two terms in the RHS of Eq. (2.6) emanate from the baroclinic term appearing in the RHS of Eq. (2.2), and points in the negative y direction, in agreement with the definition of q . As already mentioned, vorticity can be generated from two baroclinic sources:

(i) $T_1 \equiv -(g/\bar{\rho})\partial\rho/\partial x$: This term denotes the “Boussinesq baroclinic torque”. For example, at the warm-water–cold-water interface (thermocline), this term would be responsible for the propagation of interfacial gravity waves. In fact, it is the only baroclinic generation term present when the Boussinesq approximation is invoked.

(ii) $T_2 \equiv -(1/\bar{\rho}^2)(d\bar{\rho}/dz)(\partial p/\partial x)$: This term, which denotes the “non-Boussinesq baroclinic generation of vorticity”, arises out of the density variations in the inertial terms, and is completely independent of the gravitational effects. This term vanishes if Boussinesq approximation (which, in a simplified sense, implies $\bar{\rho} \approx \text{const.}$ in Eq. (2.6)) is invoked. Alternatively, if we assumed Boussinesq approximation from the onset, then Eqs. (2.4a)–(2.4b) would have resulted in Eq. (2.6) with $T_2 \equiv 0$.

The linearized kinematic condition at an interface (e.g. air-water free surface) is given by

$$\frac{\partial \eta}{\partial t} = w, \quad (2.7)$$

where η denotes the free surface displacement. One can combine Eqs. (2.4c) and (2.7) to obtain

$$\rho = -\eta \frac{d\bar{\rho}}{dz}. \quad (2.8)$$

Equations (2.8) and (2.6) can be combined together, yielding

$$\frac{\partial q}{\partial t} = -N^2 \frac{\partial}{\partial x} \left(\eta - \frac{p}{\bar{\rho}g} \right), \quad (2.9)$$

where $N(z) \equiv \sqrt{-(g/\bar{\rho})d\bar{\rho}/dz}$ is the Brunt-Väisälä (or buoyancy) frequency. In Fig. 1 we illustrate how the two terms in the RHS generates vorticity for stable stratification (positive N^2). The term T_1 results from the buoyancy restoring force acting to flatten a displaced

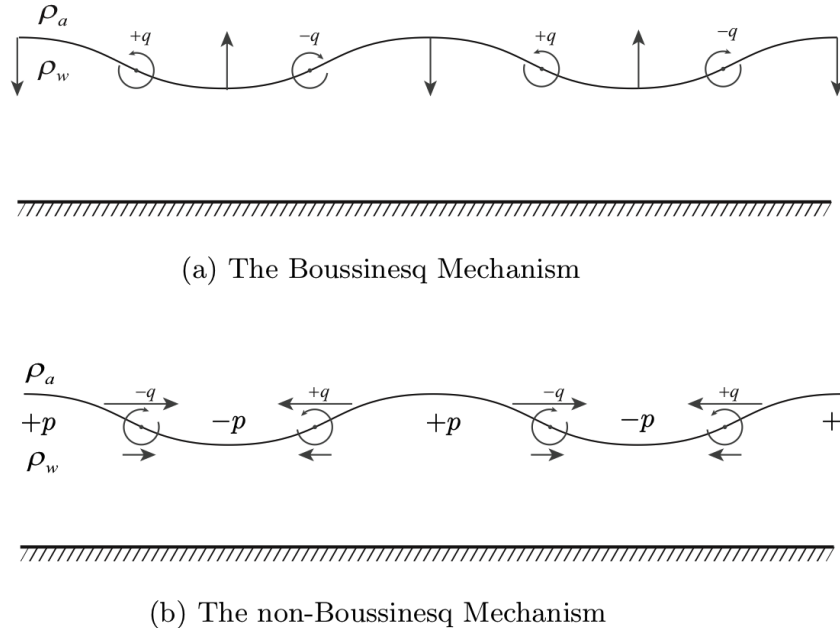


FIG. 1: Schematic illustration of the air-water interface (wavy line); density of air and water are respectively ρ_a and ρ_w . (a) The vertical arrows denote vertical velocity generated by the Boussinesq term (T_1), contributing to the $\partial w/\partial x$ in q . (b) The non-Boussinesq term (T_2) is a scaled horizontal perturbation pressure gradient force generating vertical shear of the horizontal velocity, $-\partial u/\partial z$, and thus contributes to the generation of q . In both (a) and (b), the generated q is shown by circular arrows.

density interface to its initial unperturbed horizontal position. Therefore, it generates the horizontal shear of the vertical velocity, $\partial w/\partial x$, in q ; see Fig. 1(a). The T_2 term results from the decrease with height of the mean density $\bar{\rho}$. Consequently, a horizontal perturbation pressure gradient accelerates the upper light material faster than the heavy material below it. This accounts to the vertical shear of the horizontal velocity, $-\partial u/\partial z$, in q ; see Fig. 1(b) (a more detailed analysis can be found in Heifetz and Mak¹³). Note from Eq. (2.9) that under situations when the displacement and the pressure perturbations correlate, T_1 and T_2 can act against each other in generating vorticity. This will be shown to be the case for the air-water interface – for surface gravity waves over water of finite depth, a lift up of the interface is associated with a positive density anomaly and thus with a positive pressure perturbation. Furthermore, using Eq. (2.4a) we can rewrite Eq. (2.9) as:

$$\frac{\partial}{\partial t} \left(q + \frac{N^2}{g} u \right) = -N^2 \frac{\partial \eta}{\partial x}, \quad (2.10)$$

where we note that the term T_2 is now the second term of the LHS.

A. Surface gravity waves

Let us consider the interface to be between air and water. We assume the water of depth H , while the air above it is unbounded. The origin of the coordinate system is located at the air-water interface (with z pointing vertically upwards). In this system, the mean density can be written as follows:

$$\bar{\rho}(z) = \begin{cases} \rho_a \rightarrow 0, & 0 < z < \infty, \\ \rho_w, & -H < z < 0. \end{cases} \quad (2.11)$$

In this set-up we have $N^2 = 2g\delta(z)$ (whereas, if ρ_a is not neglected, g would be replaced by the reduced gravity). This implies that the vorticity perturbation will be generated only at the air-water interface, giving rise to an undulating vortex sheet. We wish to describe the gravity wave dynamics solely from the vorticity dynamics of this interface. For modal solution of the form:

$$q = \hat{q}_0 \delta(z) e^{ik(x-ct)}, \quad (2.12)$$

(where the subscript ‘0’ indicates evaluation at $z = 0$) we can invert the vorticity to obtain the streamfunction $\psi = \nabla^{-2}q$ to express the velocity field

$$(u, w) = \left(-\frac{\partial}{\partial z}, \frac{\partial}{\partial x} \right) \psi.$$

Using the Green function approach we can write:

$$\psi = \nabla^{-2}q = \int_{-H}^{\infty} q G(z, z', k) dz' = \hat{q}_0 G(z, 0, k) e^{ik(x-ct)} = \hat{\psi}(z) e^{ik(x-ct)}, \quad (2.13)$$

where the Green function G should satisfy the Helmholtz-Poisson’s equation:

$$\left(-k^2 + \frac{\partial^2}{\partial z^2} \right) G(z, 0, k) = \delta(z), \quad (2.14)$$

together with the free boundary condition of $w(z \rightarrow \infty) \rightarrow 0$, and the solid impenetrable boundary condition, $w(z = -H) = 0$, implying $G(z = \infty; -H, 0, k) = 0$. The dynamics finally boils down to finding the modal solution that simultaneously satisfies Eq. (2.7) and Eq. (2.10) at the interface:

$$c = \frac{i}{k} \frac{\hat{w}_0}{\hat{\eta}_0}; \quad c = \frac{2g\hat{\eta}_0}{\hat{q}_0 + 2\hat{w}_0}, \quad (2.15a,b)$$

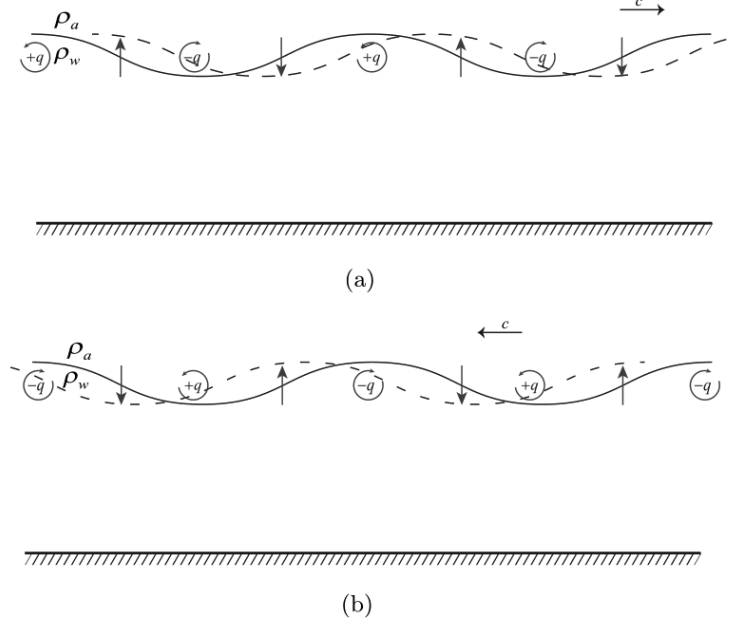


FIG. 2: Schematic illustration of the propagation of surface gravity waves. (a) When the interface vorticity (indicated by circular arrows) and displacement (indicated by the solid undulating line) are in phase, the vertical velocity (indicated by the vertical arrows) induced by the perturbation vorticity is located a quarter of wavelength to the right of the displacement, thus translating the displacement (the dashed undulating line) in the positive x direction (Eq. (2.15a)). (b) Same as in (a), except that now the wave propagates in the negative x direction as the vorticity and the displacement anomalies are in anti-phase.

where both (\hat{u}_0, \hat{w}_0) are expressed in terms of \hat{q}_0 . Equation (2.15a) reveals that for waves propagating in the positive (negative) x direction, the vertical velocity is located a quarter of wavelength to the right (left) of the displacement anomaly (see Fig. 2), whereas Eq. (2.15b) indicates that $(q_0 + 2u_0)$ and η_0 should be in phase (anti-phase) for positive (negative) wave propagation. While the former is a general property of any transverse wave, the latter will be clarified in the next section.

III. DISPERSION RELATION ANALYSIS

A. deep-water limit

Let us first consider the deep-water (hereafter DW) limit, that is, $kH \rightarrow \infty$. In this case, the Green function $G_{DW} = -e^{-k|z|}/2k$, which yields

$$\left[\psi = -\frac{\hat{q}_0}{2k} e^{-k|z|} e^{ik(x-ct)} \right]_{DW} . \quad (3.1)$$

In Fig. 3 the velocity field associated with ψ_{DW} is plotted. The evanescent structure of the vector field away from the interface shows that both divergence and vorticity fields are zero everywhere ($\partial u/\partial x = -\partial w/\partial z$ and $\partial w/\partial x = \partial u/\partial z$) except at the interface, where vorticity goes to infinity in magnitude since the jump in the sign of u across the interface generates the vortex sheet. Since $u(0^-) = -u(0^+)$, we have $u_0 = 0$. This implies that the non-Boussinesq baroclinic torque term in Eq. (2.10) vanishes in the DW limit. Furthermore, from Eq. (3.1) we obtain, $\hat{w}_0 = -i\hat{q}_0/2$, thus Eq. (2.15a,b) gives the familiar DW phase speed relation:

$$\left[c = \frac{\hat{q}_0}{2k\hat{\eta}_0} = \frac{2g\hat{\eta}_0}{\hat{q}_0} = \pm \sqrt{\frac{g}{k}} \right]_{DW} , \quad (3.2)$$

corresponding to:

$$\left[\left(\frac{\hat{q}_0}{\hat{\eta}_0} \right)^\pm = \pm 2\sqrt{gk} \right]_{DW} . \quad (3.3)$$

Hence, when the interface displacement and vorticity are in (anti) phase the wave propagates to the (left) right (see Fig. 3). Such behavior is common with other types of interfacial vorticity waves such as capillary¹⁴, Rossby¹⁵ and Alfvén¹⁶ waves.

We note a point of crucial importance – although we are considering a “non-Boussinesq” density jump (air-water interface), the non-Boussinesq effect is completely absent for the deep-water limit. In other words, this implies that the Boussinesq effects are not confined to “small density variations”, as is conventionally understood. A conclusion similar to ours is given in Guha and Raj¹⁷ using scaling arguments.

B. Finite depth

As already mentioned, our goal is to describe surface gravity waves dynamics from the vortex sheet dynamics of the air-water interface. This is straight-forward in the deep-water

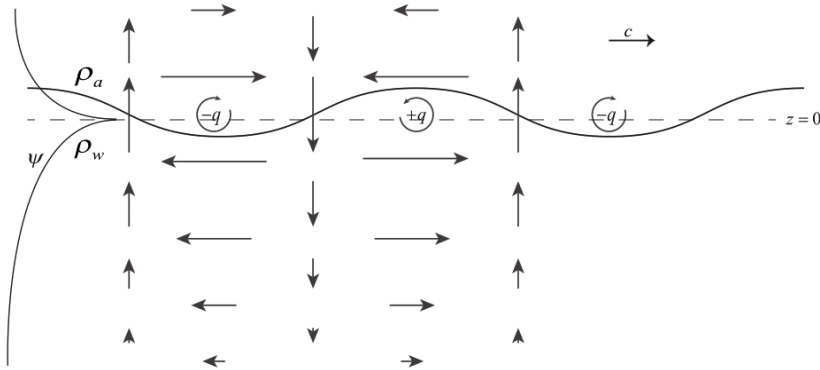


FIG. 3: The velocity field of the rightward propagating surface gravity wave in the deep-water limit. The vertical structure of the deep-water streamfunction (Eq. (3.1)) is illustrated in the left. Due to its evanescent structure away from the interface, the flow is everywhere non-divergent. It is also irrotational everywhere except at the interface, where the jump in the horizontal velocity across the interface generates a delta function in vorticity. For leftward propagating waves in the deep water limit, the velocity field is the same but the displacement is in anti-phase with the vorticity anomaly.

limit (or infinite depth case), as shown in Sec. III A. In the finite depth case, we have to capture the effect of the impenetrability of the solid boundary located at a finite distance ($z = -H$). We have captured the effect of this solid boundary by putting an anti-phased undulating vortex sheet (mirror image of the one at $z = 0$) located at $z = -2H$. This yields

$$\psi = -\frac{\hat{q}_0}{2k} (e^{-k|z|} - e^{-k|z+2H|}) e^{ik(x-ct)}, \quad (3.4)$$

which indeed vanishes at $z = -H$, satisfying impenetrability. Furthermore, this anti-phased mirror vortex sheet reduces the vertical velocity at the interface at $z = 0$ as it induces an evanescent vertical velocity of opposite sign (see Fig. 4):

$$\hat{w}_0 = -i\frac{\hat{q}_0}{2} (1 - e^{-2kH}). \quad (3.5)$$

We readily observe that when $kH \rightarrow \infty$, we recover $\hat{w}_0 = -i\hat{q}_0/2$, i.e., the vertical velocity in the deep-water limit. Due to the presence of a solid boundary at a finite depth, the phase speed should decrease according to Eq. (2.15a). This reduction in the phase speed magnitude is obtained from Eq. (2.15b) as well. Indeed, as illustrated in Fig. 4, the anti-phased mirror image vortex sheet at $z = -2H$ induces a horizontal velocity u which is

in phase with the vortex sheet at $z = 0$. In fact, the sole contribution to u_0 is from the anti-phased mirror image vortex sheet. From Eq. (3.4), u_0 is found to be

$$u_0 = - \left(\frac{\partial \psi}{\partial z} \right)_{z=0} = \frac{\hat{q}_0}{2} e^{-2kH}. \quad (3.6)$$

The above equation indicates that the vorticity production by the interface displacement becomes smaller when the non-Boussinesq term is taken into account. Stated differently, the two terms in the RHS of Eq. (2.9) work against each other (while the first Boussinesq term T_1 dominates the second non-Boussinesq term T_2), since now the interface displacement correlates with the pressure perturbation there (c.f. Fig. 1 and Fig. 4). Substituting (\hat{u}_0, \hat{w}_0) in Eq. (2.15a,b) gives

$$c = \frac{\hat{q}_0}{2k\hat{\eta}_0} (1 - e^{-2kH}) = \frac{2g\hat{\eta}_0}{\hat{q}_0 (1 + e^{-2kH})} = \pm \sqrt{\frac{g}{k} \tanh(kH)}, \quad (3.7)$$

corresponding to:

$$\left(\frac{\hat{q}_0}{\hat{\eta}_0} \right)^\pm = \pm 2 \sqrt{\frac{gk}{1 - e^{-4kH}}}. \quad (3.8)$$

Equation (3.7) is the familiar dispersion relation of intermediate depth surface gravity waves.

C. shallow-water limit

The shallow-water (hereafter SW) limit of $kH \ll 1$ is also interesting to analyze from this perspective. The vertical structure of the streamfunction becomes independent of the wavenumber when the vortex sheet and its anti-phased mirror image become very close to each other, thereby generating a series of dipole-like structures (Fig. 5). This reflects in the phase speed, which now becomes independent of the wavenumber. As can be seen from Eq. (3.4), under the shallow-water limit

$$\left[\psi = \frac{\hat{q}_0}{2} (|z| - |z + 2H|) e^{ik(x-ct)} \right]_{SW}, \quad (3.9)$$

yielding $(\hat{u}_0, \hat{w}_0) = (\frac{1}{2}, -ikH)\hat{q}_0$. Substitution of this in Eq. (2.15a,b) gives

$$\left[c = H \frac{\hat{q}_0}{\hat{\eta}_0} = g \frac{\hat{\eta}_0}{\hat{q}_0} = \pm \sqrt{gH} \right]_{SW}, \quad (3.10)$$

corresponding to:

$$\left[\left(\frac{\hat{q}_0}{\hat{\eta}_0} \right)^\pm = \pm \sqrt{\frac{g}{H}} \right]_{SW}. \quad (3.11)$$

Again, one can easily recognize that Eq. (3.10) is the familiar dispersion relation for shallow-water waves.

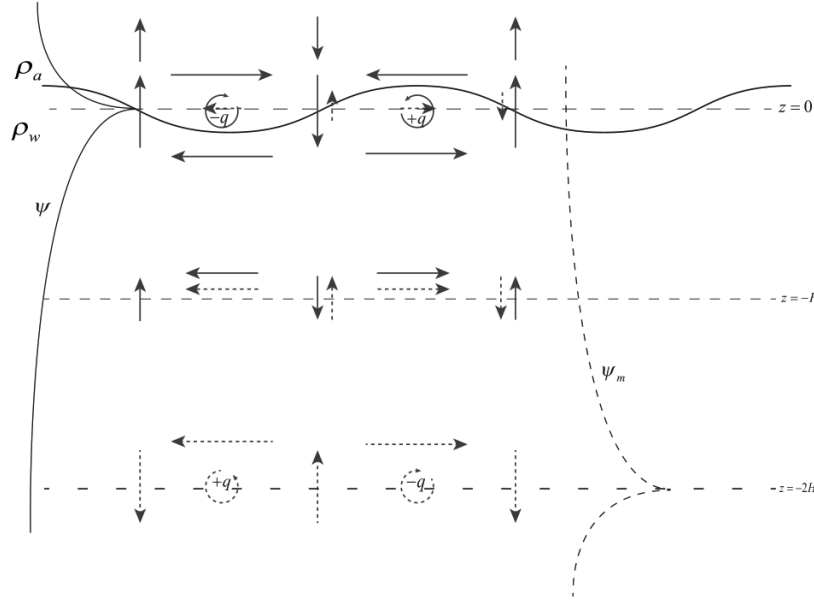


FIG. 4: Same as in Fig. 3 but for the finite depth case. Here, the velocity field results from Eq. (3.4), which is the superposition of the deep-water streamfunction (indicated in Fig. 3 by the solid evanescent profile on the left) and its anti-phase mirror image streamfunction ψ_m , whose evanescent structure away from $z = -2H$ is shown on the right with dashed line. The superposition of the induced vertical velocity from the air-water interface and its mirror image completely cancel each other at $z = -H$, thereby satisfying impenetrability. Moreover, the vertical velocity induced by the mirror image on the interface at $z = 0$ is in anti-phase with the local self-induced vertical velocity. Therefore, according to Eq. (2.15a)

and the illustration in Fig. 2, this slows the interface propagation. Furthermore, the horizontal velocity at the interface is non-zero (unlike the deep-water case) since it has a contribution from the mirror image, which is in phase with the vorticity anomaly at the interface. This stands in agreement with Eq. (2.15b) as it decreases the phase speed magnitude. The latter effect is due to the non-Boussinesq baroclinic torque (c.f. Eqs. (2.9)–(2.10) and Fig. 1b).

IV. GRAVITY WAVE ENERGY FROM THE INTERFACIAL FIELDS

Defining $K \equiv \bar{\rho}(u^2 + w^2)/2$ as the kinetic and $P \equiv \bar{\rho}(N\eta)^2/2$ as the potential energies, it is straightforward to deduce from Eqs. (2.4a)–(2.4d) that

$$\frac{\partial}{\partial t} \langle K \rangle = - \langle w \rho g \rangle = - \frac{\partial}{\partial t} \langle P \rangle, \quad (4.1)$$

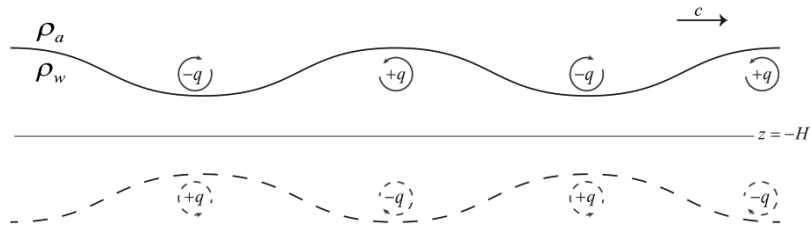


FIG. 5: The wave structure for the shallow-water limit can be viewed as a series of dipole-like bulges due to the vorticity interface and its anti-phased mirror image. In this illustration the interface anomaly is highly exaggerated in order to show the effect. When the wave propagates to the right (as shown here), the positive vorticity anomaly is above the negative one within the bulges. For leftward propagation (not shown here) the structure is upside down.

where the domain integration operator is defined as:

$$\langle \dots \rangle \equiv \frac{1}{\lambda} \int_x^{x+\lambda} \int_{z=-H}^{\infty} (\dots) dz dx, \quad (4.2)$$

where $\lambda = 2\pi/k$ is the wavelength. Equation (4.1) indicates that the total wave energy $\langle E \rangle = \langle K + P \rangle$ is conserved. After integration by parts it can be shown that

$$\langle K \rangle = -\frac{1}{2} \left\langle \psi \left(\bar{\rho} q - \frac{d\bar{\rho}}{dz} u \right) \right\rangle. \quad (4.3)$$

Substituting Eqs. (2.12), (3.4) and (3.6) we obtain

$$\langle K \rangle = \frac{\rho_w}{16k} (1 - e^{-4kH}) \hat{q}_0^2, \quad (4.4)$$

and using Eq. (3.8) we obtain the familiar result

$$\langle K \rangle = \frac{1}{4} \rho_w g \hat{\eta}_0^2. \quad (4.5)$$

Finally, substituting $N^2 = 2g\delta(z)$ in $P \equiv \bar{\rho}(N\eta)^2/2$ we recover the well known equi-partition energy relation: $\langle K \rangle = \langle P \rangle$, as demanded by the Virial theorem.

V. DISCUSSION

In this paper, we first obtain an alternative derivation for the surface gravity waves' dispersion relation, which suggests that the propagation mechanism relies only on the interfacial dynamics. The interplay between the interface displacement and the local velocity

field is crucial – the vertical velocity translates the interfacial displacement and in turn, the displacement gradient translates the combination of vorticity and horizontal velocity. The velocity field can be completely deduced by inverting the interfacial vorticity; the vanishing of the vertical velocity at the impenetrable bottom boundary can be replaced by an anti-phased mirror image of the interfacial vorticity wave. The superposition with the anti-phased image vortex sheet explains the attenuation of the phase speed due to the presence of a solid boundary. Somewhat similar to the Boussinesq, infinite scale height limit in a continuously stratified flow, the deep-water limit in the present case turns the gravity wave dynamics into a Boussinesq one. The interfacial vorticity delta function plays a central role in the dynamics – the air-water density jump across the interface generates a baroclinic torque that is concentrated only at this interface. We show that the integrated wave energy can be evaluated solely from the dynamical fields at the interface.

Finally, our analysis also provides a deeper insight into the validity and interpretation of the celebrated Boussinesq approximation. Although the conventional notion is that Boussinesq approximation is only applicable for ‘small density variations’, we conclusively show that Boussinesq approximation fully holds even for extremely strong density jumps, for example, the air-water interface, provided, we are considering the deep-water limit. In this limit, there is no effect of the density variation on the inertial terms (i.e., $T_2 = 0$), because the horizontal perturbation pressure gradient, $\partial p/\partial x$ in T_2 becomes negligible as the deep-water limit is approached. Conversely, $\partial p/\partial x$ becomes strong as the water-depth decreases, that is, as the shallow-water limit is approached. This can be intuitively understood from the fact that shallow-water flows are hydrostatic, implying that at $z = 0$, $\partial p/\partial x \propto \partial \eta/\partial x$, as shown in Fig. 1(b). Due to this finite pressure gradient, T_2 contributes to the non-Boussinesq vorticity generation.

Acknowledgments We are very grateful to Jeff Carpenter for insightful comments. A.G. gratefully acknowledges Alexander von Humboldt research fellowship for funding support.

REFERENCES

- ¹A. D. Craik, “The origins of water wave theory,” *Annu. Rev. Fluid Mech.* **36**, 1–28 (2004).

- ²P. K. Kundu, I. M. Cohen, and D. R. Dowling, “Fluid mechanics,” (2016).
- ³J. Holmboe, “On the behavior of symmetric waves in stratified shear layers,” *Geophys. Publ* **24**, 67–113 (1962).
- ⁴S. Sakai, “Rossby-Kelvin instability: a new type of ageostrophic instability caused by a resonance between Rossby waves and gravity waves,” *J. Fluid Mech.* **202**, 149–176 (1989).
- ⁵P. G. Baines and H. Mitsudera, “On the mechanism of shear flow instabilities,” *J. Fluid Mech.* **276**, 327–342 (1994).
- ⁶C.-C. P. Caulfield, “Multiple linear instability of layered stratified shear flow,” *J. Fluid Mech.* **258**, 255–285 (1994).
- ⁷E. Heifetz, C. H. Bishop, and P. Alpert, “Counter-propagating Rossby waves in the barotropic Rayleigh model of shear instability,” *Q. J. R. Meteorol. Soc.* **125**, 2835–2853 (1999).
- ⁸E. Heifetz and J. Methven, “Relating optimal growth to counterpropagating Rossby waves in shear instability,” *Phys. Fluids* **17**, 064107 (2005).
- ⁹J. R. Carpenter, E. W. Tedford, E. Heifetz, and G. A. Lawrence, “Instability in stratified shear flow: Review of a physical interpretation based on interacting waves,” *Appl. Mech. Rev.* **64**, 060801–17 (2013).
- ¹⁰A. Guha and G. A. Lawrence, “A wave interaction approach to studying non-modal homogeneous and stratified shear instabilities,” *J. Fluid Mech.* **755**, 336–364 (2014).
- ¹¹We define any linear interfacial wave that propagates due to vorticity anomalies across the interface as a vorticity wave. Hence Rossby waves, gravity waves, capillary waves, Alfvén waves are all vorticity waves by our definition.
- ¹²D. Bhardwaj and A. Guha, “Nonlinear modeling of stratified shear instabilities, wave breaking, and wave-topography interactions using vortex method,” *Phys. Fluids* **30**, 014102 (2018).
- ¹³E. Heifetz and J. Mak, “Stratified shear flow instabilities in the non-Boussinesq regime,” *Phys. Fluids* **27**, 086601 (2015).
- ¹⁴L. Biancofiore, E. Heifetz, J. Hoepffner, and F. Gallaire, “Understanding the destabilizing role for surface tension in planar shear flows in terms of wave interaction,” *Phys. Rev. Fluids* **2**, 103901 (2017).
- ¹⁵B. J. Hoskins, M. E. McIntyre, and A. W. Robertson, “On the use and significance of isentropic potential vorticity maps,” *Quarterly Journal of the Royal Meteorological Society*

111, 877–946 (1985).

¹⁶E. Heifetz, J. Mak, J. Nycander, and O. M. Umurhan, “Interacting vorticity waves as an instability mechanism for magnetohydrodynamic shear instabilities,” *J. Fluid Mech.* **767**, 199–225 (2015).

¹⁷A. Guha and R. Raj, “On the inertial effects of density variation in stratified shear flows,” *Phys. Fluids* **30**, 126603 (2018).